# Brillouin scattering measurements on optical glasses

D. Heiman, D. S. Hamilton, and R. W. Hellwarth
*Department of Physics, University of Southern California, University Park, Los Angeles, California 90007*
(Received 10 January 1979)

The room-temperature Brillouin spectra of 16 optical glasses of varying composition have been measured. Sound velocities for both transverse and longitudinal waves were determined along with the Pockels electro-optic coefficients $p_{12}$ and $p_{44}$. The damping parameter for the longitudinal phonons was obtained from linewidth measurements. The linewidths varied from 0.05 to 0.30 GHz full width at half maximum (FWHM) but averaged about 0.2 GHz, which is much larger than that in most normal crystalline materials. All spectra were recorded with a minicomputer-controlled triple-pass plane Fabry-Perot interferometer. The active alignment stabilization by computer control is discussed. Our experimental results indicate that there is at most a weak correlation between the hypersound parameters and the glass composition or other physical parameters. The frequency dependence of the damping in pure silica and the dense lanthanum flint glass LaSF-7 was measured. For these two glasses, a damping of the form $\gamma \alpha f^m$ was fit to the data, where $m \simeq 1$ for LaSF-7 and $m = 2.7 \pm 0.2$ for pure silica. Simple phenomenological models of damping by relaxation processes indicate that the relaxation rate $\tau^{-1}$ at room temperature (in LaSF-7) is about 1 $cm^{-1}$, whereas in pure silica $\tau^{-1} >> 1$ $cm^{-1}$. Also, in pure silica the frequency dependence is anomalously strong since all models predict $m \leq 2$.

## I. INTRODUCTION

In condensed media, thermally excited sound waves produce fluctuations in the refractive index via the stress-optic effect. Brillouin scattering occurs when light is Bragg reflected from this moving index "grating." Spectral measurement of the Doppler shifted light determines the velocity and attention of these sound waves, while the magnitude of the scattered light gives values for the elasto-optic or Pockels photoelastic coefficients.

The Brillouin scattering spectrum of amorphous solids consists of five main components, two frequency shifted doublets and a strong unshifted central component. The central feature is orders-of-magnitude stronger and is much narrower spectrally than the shifted doublets. Each doublet consists of Stokes (downshifted) and anti-Stokes (upshifted) components, shifted equally in frequency from the monochromatic beam being scattered. There are two of these doublets because both shear and compressional restoring forces exist in a solid. These waves produce an oscillating density modulation, in time and space, that travels with some characteristic velocity $v$. Light of frequency $\nu$ scattered or Bragg reflected from these propagating fluctuations will suffer a Doppler shift to the frequency of $\nu \pm f$. The frequency shift $f$ is given by

$$f = \frac{vn}{\lambda_0} 2 \sin(\tfrac{1}{2}\theta) \ , \tag{1}$$

where $n$ is the refractive index, $\lambda_0$ is the incident light wavelength in vacuum, and $\theta$ is the angle between the incident and scattered optical wave vectors. The spectral width $\gamma$ [full width at half maximum (FWHM): in Hertz] of each feature is related to the acoustic-wave power attenuation coefficient

$$\beta = 2\pi\gamma/v \ . \tag{2}$$

The first observation of the Brillouin lines in amorphous materials was made in 1950 by Krishnan[1] in pure silica. In 1959, Flubacher *et al.*[2] were the first to observe both doublets corresponding to transverse and longitudinal sound waves. Since then, laser light sources have been used to determine the temperature dependence of the Brillouin lines in pure silica. Pine[3] measured the velocity and linewidths below room temperature while Bucaro and Dardy[4] and Pelous and Vacher[5] made measurements at high temperatures. The temperature dependence of the elasto-optic constants has been determined at high temperature[4] and the damping of the transverse waves has been measured below room temperature.[6] The temperature dependence of the damping of the longitudinal waves has been determined for different frequencies at low temperatures.[7]

The intensity of the unshifted central component in the Brillouin spectrum of amorphous solids can be many orders of magnitude larger than the shifted components. The transverse peaks are usually 10 to

 

TABLE I. Designation of glass sample materials.

| | |
|---|---|
| $SiO_2$: | Homosil vitreous quartz (Amersil, Inc.) |
| BK-3: | BSC-3 borosilicate crown (Hoya, Inc.) having the composition (wt.%): 71 $SiO_2$, 14 $B_2O_3$, 10 $Na_2O$, 5 $Al_2O_3$ (Ref. 29). |
| BK-7: | BSC-7 borosilicate crown having the composition (wt%): 69.6 $SiO_2$, 9.9 $B_2O_3$, 8.4 $Na_2O$, 8.4 $K_2O$, 2.5 BaO (Ref. 29). |
| ED-2: | ED-4 silicate glass doped nominally with 3wt%Nd. |
| ED-4: | Silicate glass undoped, having the composition (mol%) 60 $SiO_2$, 27.5 $Li_2O_3$, 10 CaO, 2.5 $Al_2O_3$. |
| ED-8: | Silicate glass doped with Nd (similar to ED-2) |
| SF-6: | FD-6 alkali-lead-silicate glass (Hoya, Inc.) having the composition (wt%): 27.3 $SiO_2$, 1.5 $K_2O$, 71.0 PbO (Ref. 29) |
| SF-7: | (Schott) Alkali-lead-silicate glass |
| LaSF-7: | Dense lanthanum flint (Schott) containing mostly $B_2O_3$, $La_2O_3$ and $ThO_2$ with a few % $Ta_2O_5$ and $Nb_2O_5$. |
| TaF-1: | Tantalum flint (Hoya, Inc.) |
| LHG-5: | Doped phosphate glass with 0.3 wt% Nd (Hoya, Inc.) |
| LHG-6: | Doped phosphate glass with 0.3 wt% Nd (Hoya, Inc.) |
| P-224: | Doped phosphate glass with 4.8 wt% $Nd_2O_3$. |
| L-248: | Doped fluorophosphate glass having the molar composition: 16% Al $(PO_3)_3$; 50% LiF, 33% NaF; 1% $Nd_2O_3$. |
| FK-51: | Undoped fluorophosphate having the composition (mol%): 23.4 $SrF_2$, 18.7 $AlF_3$, 16.2 $CaF_2$, 12.4 LiF, 11.9 $BaF_2$, 6.9 $Al(PO_3)_3$, 2.0 $Al_2O_3$ and 0.6 NaF. |
| FK-5: | FC-5 fluoro crown (Hoya, Inc.) |

100 times smaller than the longitudinal peaks. Thus, the central component can be as much as $10^5$ times larger than the transverse peaks. In order to resolve these weak features a frequency analyzer with high contrast is required. A computer-stabilized triple-pass plane Fabry-Perot interferometer facility is described and was used to collect the Brillouin spectra. Also, a convenient method to remove the broadening of the Brillouin peaks caused by the instrumental resolution is discussed.

Brillouin scattering measurements at room temperature in a wide variety of glass types are presented here. The glass types include pure silica, light silicates, heavy-metal silicates, phosphate, fluorophosphate, and fluoroberyllates. The compositions or major constituents are listed in Table I. The sound velocities are determined and are used to determine the elastic properties, while the scattered light intensities are used to determine the elasto-optic constants. The linewidths of the longitudinal peaks are measured in order to determine the sound-wave damping rates. The linewidths in two samples are measured for different peak frequencies to determine the frequency-dependent damping. Finally, models for damping are examined in order to fit the frequency dependence.

## II. BACKGROUND

### A. Brillouin scattering theory and elastic properties

In an isotropic solid, the power $I_{\alpha\beta}$ of light scattered from polarization $\alpha$ to polarization $\beta$ per unit solid angle, for both doublet elements of longitudinal-acoustic (LA) phonons is[8,9]

$$I_{VV} = I_0 V_s \pi^2 kT \frac{\epsilon^4}{\lambda_0^4} \frac{|p_{12}|^2}{\rho v_L^2} \quad , \tag{3}$$

$$I_{HH} = I_0 V_s \pi^2 kT \frac{\epsilon^4}{\lambda_0^4} \frac{1}{\rho v_L^2} |p_{44} + (p_{12} + p_{44}) \cos\theta|^2 \quad , \tag{4}$$

and by the transverse-acoustic (TA) phonons is

$$I_{VH} = I_{HV} = I_0 V_s \pi^2 kT \frac{\epsilon^4}{\lambda_0^4} \frac{|p_{44}|^2}{\rho v_T^2} \cos^2(\tfrac{1}{2}\theta) \quad , \tag{5}$$

where $V$ and $H$ refer to vertical and horizontal relative to a horizontal scattering plane. The incident light intensity is $I_0$, the scattering volume is $V_s$, $kT$ is the thermal phonon energy, $\rho$ is the mass density, $v_T$ and $v_L$ are the transverse and longitudinal sound velocities, respectively, and $p_{ij}$ are the Pockels elasto-optic coefficients. Since the scattering arises from the fluctuations in the dielectric constant $\epsilon$, which ultimately comes from strains produced by sound waves, the electro-optic coefficients in a cubic material are defined by

$$\delta(\epsilon^{-1})_{ij} \equiv \sum_{kl} p_{ijkl} S_{kl} \quad . \tag{6}$$

Here, the strain tensor components $S_{kl}$ are related to the elastic deformation components $u_k$, along the coordinate axes $x_k$ by

$$S_{kl} = \tfrac{1}{2}(\partial u_k/\partial x_l + \partial u_l/\partial x_k) \quad .$$

In the case of an isotropic solid there are only two independent coefficients $p_{12}$ and $p_{44}$. Equation (6) now reduces to

$$\delta\epsilon_{ij} = -\epsilon^2 \left[ 2p_{44} S_{ij} + p_{12} \left( \sum_k S_{kk} \right) S_{ij} \right] \quad . \tag{7}$$

The Pockels constants are related to the change in the dielectric constant caused by a change in hydrostatic compression according to[10]

$$\frac{\delta\epsilon}{\delta\rho} = \frac{\epsilon^2}{\rho} (p_{12} + \tfrac{2}{3} p_{44}) \quad . \tag{8}$$

In a liquid where there is no shear restoring force, $p_{44}$ is zero and Eq. (8) becomes

$$\epsilon p_{12} = \partial \ln(\epsilon)/\partial \ln(\rho) \quad .$$

The simplest way to determine the sound velocities and relative elasto-optic constants is to employ a 90° scattering angle. For this right-angle scattering geometry, the differential scattering efficiency, per unit solid angle $\Omega$, per phonon sideband as defined by $dh/d\Omega = 1/V_s(I/I_0)$, from Eqs. (3)–(5) simplify to

$$\left( \frac{dh}{d\Omega} \right)_{VV} = \frac{\pi^2 kT \epsilon^4}{2\lambda_0^4} \frac{|p_{12}|^2}{\rho v_L^2} \quad , \tag{9}$$

$$\left( \frac{dh}{d\Omega} \right)_{HH} = \frac{\pi^2 kT \epsilon^4}{2\lambda_0^4} \frac{|p_{44}|^2}{\rho v_L^2} \quad , \tag{10}$$

for LA phonons, and

$$\left( \frac{dh}{d\Omega} \right)_{VH,HV} = \frac{\pi^2 kT \epsilon^4}{4\lambda_0^4} \frac{|p_{44}|^2}{\rho v_T^2} \tag{11}$$

for TA phonons. Thus, in this geometry, the TA peaks appear in both $VH$ and $HV$ equally, while the LA peaks appear in $VV$ and $HH$ with different strengths. Normally, in glasses, $p_{12}$ is somewhat larger than $p_{44}$, hence the LA peaks in $VV$ are much larger than in the $HH$ configuration. We also note that the TA peaks are strongest at 90° scattering and decrease for larger or smaller angles.

The elastic constants in an isotropic solid are defined in terms of the elastic quantities, Young's modulus, shear modulus, bulk modulus, and Poisson ratio, respectively, by[11]

$$Y_0^{\text{ad}} = C_{44} \left( \frac{3C_{11} - 4C_{44}}{C_{11} - C_{44}} \right) \quad , \tag{12}$$

$$\mu^{\text{ad}} = C_{44} \quad , \tag{13}$$

$$B = C_{11} - \tfrac{4}{3} C_{44} \quad , \tag{14}$$

$$\sigma = \frac{Y_0}{2\mu} - 1 \quad , \tag{15}$$

where the superscript implies it is the adiabatic value determined at high frequencies.

### B. Attenuation of sound waves

The sound-wave attenuation in amorphous materials is generally intermediate between that of crystalline solids and liquids.[12] In liquids, the phonon linewidth is large because of the extra degrees of freedom compared to that of solids. In crystalline solids the linewidths are usually less than about 50 MHz at Brillouin frequencies, but can become very large due to anharmonic decay near critical phase transitions[7] or when mode coupling occurs.[13,14] The process of heat conduction can only account for a small percentage of the sound attenuation in dielectrics. Bommel and Dransfeld[15] have used a model introduced by Akheizer[16] to successfully correlate the attenuation with the phonon anharmonicity in crystals. In $\alpha$-quartz the attenuation was calculated

from the Gruneisen constant which measures the macroscopic anharmonicity, and the relaxation time computed from thermal conductivity. In amorphous solids the attenuation is much larger than that calculated from the Gruneisen constant and hence is anomalous in this respect.[17]

The sound-wave damping in pure silica has a peak at low temperature which is due to a resonant condition between the sound-wave frequency and the temperature-dependent relaxation rate[18] $\tau^{-1}$. For sound-wave frequencies $\omega \lesssim \tau^{-1}$ the damping is described quite well by structural relaxation due to two-level systems.[19]

The frequency dependence of the sound-wave damping $\gamma$ in amorphous materials has been described considering anharmonic interactions[3] and also a structural relaxation.[18] Both models predict

$$\gamma(\omega,T)=\sum_j A_j \frac{\omega^2\tau_j(T)}{1+\omega^2\tau_j^2(T)} \quad , \tag{16}$$

where $\omega$ is the frequency of the sound wave, $A$ is the relaxation strength, and $\tau^{-1}$ is the characteristic relaxation rate. The indicated summation includes effects from more than one discrete relaxation process or a continuous distribution of relaxation rates.[18]

The relaxation rate can be strongly temperature dependent below room temperature, but is usually taken to be frequency independent. In the structural relaxation model the temperature dependence is described by either the Arrhenius form $\tau^{-1}(T) = \tau_0^{-1}e^{-E/kT}$ for very low temperatures or the Eyring form $\tau^{-1}(T)=(kT/h)e^{-E/kT}$. Here $E$ is the activation energy for jumping the barrier between two potential-energy minima that describe the structural configurations. The anharmonic decay model uses

$$\tau^{-1}(T)=\tau_0^{-1}(n''+n'+1)$$

or

$$\tau^{-1}(T)=\tau_0^{-1}(n''-n')$$

for phonon decay or scattering processes, respectively, where the thermal occupation numbers $n'$ and $n''$ are computed using the energies of the participating phonons.

In order to examine the frequency dependence of Eq. (16) more easily, the slope of the log-log plot is defined as the exponent $m$ assuming $\gamma\alpha\omega^m$. For the simple case of a single relaxation process

$$m=\frac{2}{(1+\omega^2\tau^2)} \quad . \tag{17}$$

Thus, at low frequencies, $\omega << \tau^{-1}$, there is a quadratic dependence; at intermediate frequencies, $\omega \simeq \tau^{-1}$, there is a linear dependence; and for very high frequencies $\omega >> \tau^{-1}$ the damping is frequency independent. Experimentally, the frequency dependence will provide information on the relaxation rate for the largest contribution to sound-wave damping.

## III. EXPERIMENTAL APPARATUS

The Brillouin scattering spectra of glasses was recorded with the triple-pass Fabry-Perot interferometer facility diagrammed in Fig. 1. This system included a single-mode argon-ion laser, a monochromator to reject excess scattered light, a scanning Fabry-Perot interferometer to frequency analyze small-frequency-shift light, and a minicomputer to stabilize the interferometer and accumulate data. A Burleigh Instruments RC-110 piezoelectrically scanned Fabry-Perot interferometer was fitted with corner-cube retroreflectors to allow triple passing. The extra available spectral contrast ($\sim 10^8$), defined as the ratio of maximum transmission to minimum transmission, is needed when the nearly elastic scattering is many orders of magnitude larger than the Brillouin peaks,[20] as in glasses. A Spex 1400 double-grating monochromator was operated with a fixed bandpass usually 3 to 5 $cm^{-1}$ centered at the laser wavelength in order to reject both the high-frequency ($>50$ $cm^{-1}$) Raman scattering from vibrations and excess low-frequency (0 to 50 $cm^{-1}$) scattering that is observed in all glasses. A cooled ITT FW-130 photomultipler with phonon-counting equipment was attached to the exit slit of the spectrometer. A Hewlett-Packard 9825 desk-top calculator was interfaced to: an $X$-$Y$ plotter for hard copy data output; a CRT storage scope for temporary display of data; and the experimental apparatus by an HP 6940B multiprogrammer.

The stability and alignment constraints for a Fabry-Perot interferometer in a multipass configuration are much more severe than in single pass. With data accumulation on the order of hours, a continual alignment optimization during data collection is required. This active alignment stabilization is con-

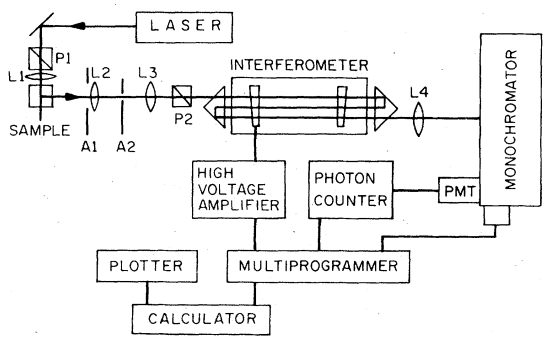


FIG. 1. Schematic diagram of the triple-pass Fabry-Perot interferometer facility. $P1$ and $P2$ are Glan polarizers, $L1$ to $L4$ are coated converging lenses with focal lengths of 150, 50, 100, and 65 mm, respectively; $A1$ is a collection angle stop aperture, and $A2$ is a pin hole aperture.

trolled by a minicomputer-based system of our own design. The computer, interfaced to the interferometer and the photon-counting hardware, performs two basic functions: scans the interferometer plate spacing and simultaneously collects photon counts, makes small tilt corrections to the Fabry-Perot plates and tests the results of these corrections in order to maximize the count rate in a narrow window around the Fabry-Perot transmission peak. Each scan must meet a minimum throughout criteria before it is added to the accumulating data array. The computer analyzes the final spectra and extracts the center frequency and width of the Brillouin peaks.

## IV. EXPERIMENTAL RESULTS

### A. Elastic and elasto-optic constants

Measurements of the elasto-optic constants and sound velocities were taken in a 90° scattering geometry as shown in Fig. 1. The 488 nm wavelength incident light was $V$ polarized while the scattered light that was accepted had both $V$ and $H$ polarizations. A typical spectrum with this geometry is shown in Fig. 2(a). The Fabry-Perot mirrors were spaced to give about a 2.5 $cm^{-1}$ free spectral range (FSR) so that both TA- and LA-phonon peaks could be observed in first order without overlapping. The finesse was about 40 while the contrast ratio was observed to be greater than $10^6$. The combined FSR and scattering angle was calibrated to within 0.5% using the LA peaks in pure silica.[3] The sound velocities were calculated from Eq. (1) using the frequency shift that is determined by measuring the position of the centroid of the scattering peak. The peak positions and hence the sound velocities have an absolute uncertainty of 1%. The integrated scattering intensity of each peak, after subtracting the background, was measured relative to the LA peak in pure silica. Corrections were made for differences in the solid angle of collection and reflection losses at the sample surfaces resulting from the refractive index differences. The Pockels electro-optic constants $p_{12}$ and $p_{44}$, relative to $p_{12}$ in pure silica, were determined for all the samples using Eqs. (9) and (11). The averaged results for the sound velocities and elasto-optic coefficients are tabulated in Table II.

All of the acoustic peaks were observed in $VV$ and $VH$ geometries except for the TA peak in SF-6. The nonappearance of this peak can result from either a very low elastic constant for shear stress, or a small value for the elasto-optic constant $p_{44}$. In $HH$ geometry the LA peak should appear with nearly the same magnitude as the TA peak in $VH$ geometry. This peak was also absent in $HH$ indicating a very small elasto-optic constant for shear waves.

The elastic constants $C_{11}$ and $C_{44}$ were determined from the sound velocities and are tabulated in Table III. Values are derived for the adiabatic constants $\mu$, $Y_0$, $\sigma$, and $B$ from the elastic constants and the formulas in Sec. II. For comparison, the isothermal values for $\mu$ and $Y_0$ are listed and were taken from the manufacture's catalogue. The differences $Y_0^{iso} - Y_0^{ad}$ and $\mu^{iso} - C_{44}$ are also listed.

The currently accepted value for $p_{12}$ in pure silica is 0.286.[21] This value was determined by measuring the scattering intensity of the Brillouin peaks of silica relative to that in a liquid of known elasto-optic constant. Similar values are found by other methods.[22,23] We have also measured the elasto-optic constant $p_{12}$ in pure silica by comparing the Brillouin intensity relative to the known integrated Raman cross section.[24] A measurement is made of the

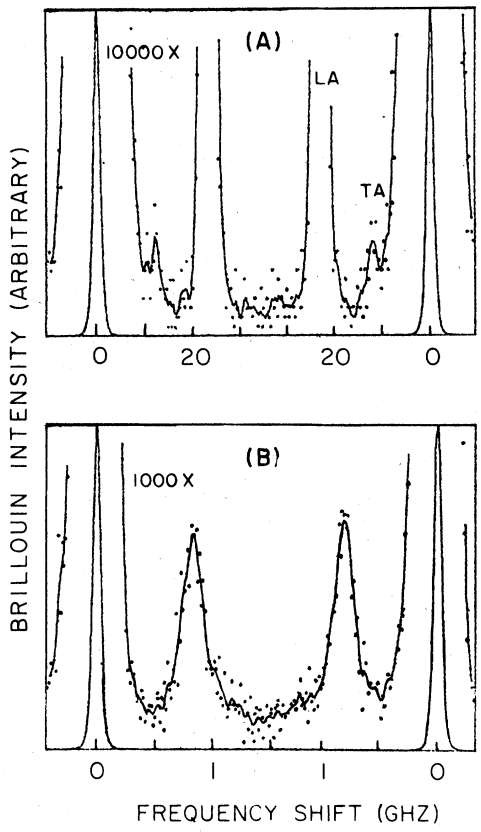


FIG. 2. Interferometer scans of the Brillouin intensity vs frequency shift for two glasses at 488 nm wavelength excitation. (a) shows both transverse-acoustic (TA) and longitudinal-acoustic (LA) phonon peaks of FK-51 glass in a right-angle scattering geometry with a free spectral range (FSR) of 69.5 GHz. The upper curve is magnified by $10^4$ and smoothed over five points. (b) shows the LA-phonon peaks of SF-6 glass in a back scattering geometry with high resolution and an FSR of 3 GHz. The upper curve is magnified by $10^3$ and smoothed over five points.

TABLE II. Results from Brillouin scattering experiments on silicate, phosphate and fluorophosphate glasses. The values given for the longitudinal-acoustic damping $\gamma$ are the full width at half maximum of the scattering peak having a frequency shift $f$.

| Glass Material | Index $n_f$ (486 nm) | Density (gm/cm$^3$) | Sound Velocity ($10^5$ cm/sec) TA | LA | $\frac{\lvert p_{44}\rvert}{\lvert p_{12}\rvert_{SiO_2}}$ | $\frac{\lvert p_{12}\rvert}{\lvert p_{12}\rvert_{SiO_2}}$ | LA Damping $\gamma$ (GHz) | $f$ (GHz) |
|---|---|---|---|---|---|---|---|---|
| $SiO_2$ (Homosil) | 1.463 | 2.21 | 3.79 | 5.92 | 0.29 | ≡1.00 | 0.17 ±0.02 | 34.7 |
| | | | (±1%) | (±1%) | (±20%) | (±10%) | (±20%) | (±3%) |
| BK-3 | 1.504 | 2.37 | 3.29 | 5.49 | 0.20 | 0.85 | 0.20 | 33.2 |
| BK-7 | 1.522 | 2.51 | 3.65 | 6.05 | 0.20 | 0.83 | 0.19 | 37.0 |
| ED-2 | 1.573 | 2.55 | 3.85 | 6.59 | 0.17 | 0.76 | 0.18 | 41.1 |
| ED-4 | 1.570 | 2.49 | 3.83 | 6.59 | 0.18 | 0.77 | 0.14 | 41.1 |
| ED-8 | 1.570 | 2.66 | 3.96 | 6.90 | 0.17 | 0.71 | 0.19 | 41.8 |
| SF-6 | 1.828 | 5.19 | · · · | 3.49 | <0.02 | 0.63 | 0.18 | 25.8 |
| SF-7 | 1.653 | 3.80 | 2.38 | 4.10 | 0.13 | 1.07 | 0.13 | 27.5 |
| LaSF-7 | 1.939 | 5.79 | 3.56 | 5.55 | 0.16 | 0.58 | 0.30 ±0.01 | 43.0 |
| TaF-1 | 1.783 | 4.50 | 3.21 | 5.99 | 0.17 | 0.78 | 0.22 | 43.7 |
| LHG-5 | 1.543 | 2.67 | 3.12 | 5.40 | 0.15 | 0.92 | 0.16 | 33.5 |
| LHG-6 | 1.536 | 2.62 | 3.28 | 5.58 | 0.15 | 0.86 | 0.24 | 34.5 |
| P224 | 1.550 | 2.71 | 3.13 | 5.49 | 0.12 | 0.72 | 0.25 | 33.9 |
| L248 | 1.479 | 2.70 | 2.99 | 5.34 | 0.11 | 0.65 | 0.13 | 31.7 |
| FK-51 | 1.495 | 3.63 | 3.09 | 5.34 | 0.05 | 0.61 | 0.05 | 32.1 |
| FK-5 | 1.492 | 2.45 | 3.17 | 5.36 | 0.20 | 0.94 | 0.29 | 31.9 |

TABLE III. Elastic constants given in $10^{10}$ dynes/cm$^2$ were derived from the sound velocity measurements of Table II. The elastic constants are determined from $C_{44}=\rho v_{TA}^2$ and $C_{11}=\rho v_{LA}^2$. The superscripts ad and iso denote adiabatic and isothermal, respectively. The moduli derived from the hypersound velocities are adiabatic while the isothermal values listed were taken from the manufacturer's catalogue and were measured at frequencies of 1–10 kHz.

| Material | $C_{11}$ ($10^{10}$ dynes)/cm$^2$ | $C_{44}$ | $Y_0^{ad}$ | $\sigma$ | $B$ | $\mu^{iso}$ | $Y_0^{iso}$ | $Y_0^{iso}-Y_0^{ad}$ |
|---|---|---|---|---|---|---|---|---|
| | ±2% | ±2% | ±3% | ±3% | ±3% | ±2% | ±2% | |
| $SiO_2$ | 77.5 | 31.7 | 73.2 | 0.155 | 35.2 | 31.0 | 71.7 | −1.5 ±3 |
| BK-3 | 71.4 | 25.7 | 62.6 | 0.218 | 37.1 | 30.8 | 74.2 | 11.6 ±3 |
| BK-7 | 91.9 | 33.4 | 81.2 | 0.216 | 47.4 | 33.7 | 81.5 | 0.3 ±3 |
| ED-2 | 111 | 37.8 | 93.9 | 0.242 | 60.6 | 36.3 | 90.1 | −3.9 ±4 |
| ED-4 | 108 | 36.5 | 90.8 | 0.244 | 59.3 | 36.3 | 90.1 | −0.7 ±4 |
| ED-8 | 127 | 41.7 | 104 | 0.259 | 71.4 | | | |
| SF-6 | ~(63) | (21) | (52) | (0.238) | (35) | 22.3 | 55.5 | (+3.5) ±4 |
| SF-7 | 63.9 | 21.5 | 53.6 | 0.247 | 35.2 | 23.0 | 56.2 | +2.6 ±2 |
| LaSF-7 | 178 | 73.4 | 169 | 0.151 | 80.1 | 51.0 | 132 | −37 ±5 |
| TaF1 | 162 | 46.4 | 120 | 0.293 | 100 | | | |
| LHG-5 | 77.9 | 26.0 | 64.9 | 0.248 | 43.2 | 25.8 | 61.3 | −3.6 ±3 |
| LHG-6 | 81.6 | 28.2 | 69.7 | 0.236 | 44.0 | | | |
| P224 | 81.7 | 26.5 | 66.9 | 0.262 | 46.4 | | | |
| L248 | 77.0 | 24.1 | 61.4 | 0.274 | 44.9 | | | |
| FK-51 | 104 | 34.7 | 86.5 | 0.246 | 57.7 | 30.6 | 78.8 | −7.7 ±3 |
| FK-5 | 70.4 | 24.6 | 60.6 | 0.232 | 37.6 | 25.7 | 62.0 | +1.4 ±2 |

$VV$ Brillouin spectrum when the Raman shifted light is also allowed to enter the detector. The spectrometer in Fig. 1 is replaced by a colored filter that has a wavelength cutoff at the long-wavelength limit of the Stokes spectrum (1500 $cm^{-1}$). The Brillouin spectrum now consists of the LA peaks on top of a large background. This background is the combined Stokes and anti-Stokes, polarized scattering. The ratio of the area of the integrated Raman spectra to that of one LA peak was found to be $2.07 \pm 0.10$. The total, polarized, Stokes plus anti-Stokes integrated scattering efficiency for pure silica from Ref. 23 is

$$15.9 \pm 0.8 \times 10^{-8}\ cm^{-1}sr^{-1}$$

at $\lambda_0 = 488$ nm. Combining these results with Eq. (9) the elasto-optic constant $p_{12}$ in pure silica was determined to be $0.283 \pm 0.020$.

### B. Acoustic-wave damping

The damping of the LA phonons was measured at room temperature and is tabulated in Table II. The phonon damping parameter $\gamma$ (full width at half maximum) is related to the acoustic attenuation constant $\alpha$ by $8.68\pi\gamma = v\alpha$, where the units are Hz for $\gamma$, cm/sec for $v$, and $db$/cm for $\alpha$. Near backscattering geometry was used in all cases with the angle adjusted such that the phonon peaks did not overlap each other or the elastic peak. The FSR was chosen between 1.5 and 3 GHz resulting in a resolution of 30 to 80 MHz. Fig. 2(b) is a typical high-resolution (3 GHz FSR) spectrum of the LA peaks in FK-51.

There are two mechanisms that broaden the intrinsic Brillouin linewidths similar to that in phonon-polariton measurements.[25] The first is inhomogeneous broadening caused by the linear phonon dispersion. The phonon frequency and wave vector are related to the scattering angle $\theta$, inside the material, by $f = vq/2\pi$ and

$$q = (4\pi n/\lambda_0)\sin(\tfrac{1}{2}\theta) \ .$$

A finite acceptance angle of $\Delta\theta$ will cause the frequency to broaden by

$$\Delta f = (vn/\lambda_0)\cos(\tfrac{1}{2}\theta) \ .$$

Therefore, the experiments were performed at large scattering angles to minimize this broadening. Collection optics of $f/50$ resulted in 5 to 10 MHz broadening in $\gamma$, computed by numerically integrating over the collecting aperture, was subtracted in each case.

The second and larger cause of linewidth broadening is due to the instrumental resolution of the interferometer. The deconvolution of the FWHM value $\gamma$ for the phonon mode from the measured FWHM value $\gamma'$ was done using the curve of Fig. 3. Here a

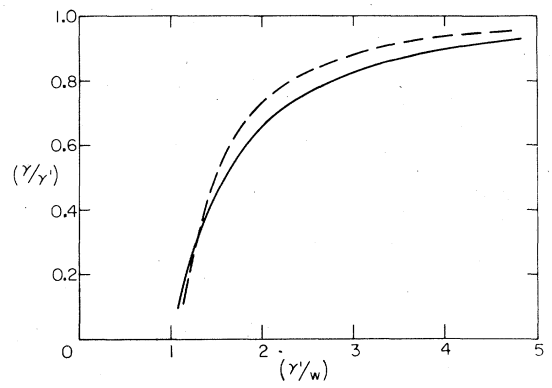


FIG. 3. Instrumental resolution broadening of the full width at half maximum (FWHM) of a Lorentzian profile. The FWHM of the unbroadened Lorentzian line shape is $\gamma$; $\gamma'$ is the broadened FWHM; and $W$ is the FWHM of the instrumental resolution. The solid line is the result of convolution of a Lorentzian with the Airy cubed resolution function of a triple-pass Fabry-Perot interferometer. For comparison, the dashed curve is the result of convolution of a Lorentzian with a triangle function appropriate to a scanning spectrometer.

Lorentzian of FWHM $\gamma$ was convoluted with the cube of an Airy function of FWHM $W$ used to represent the instrumental response function of the triple-passed Fabry-Perot. The FWHM of this numerical convolution is then $\gamma'$ and the ratio $\gamma/\gamma'$ as a function of $\gamma'/W$ is indicated in Fig. 3. The value of $W$ is taken from the FWHM of the elastic peak and $\gamma'$ from the raw data after background subtraction. The resolution broadening was removed first, then the dispersion broadening was calculated for each glass and then subtracted to yield the values in Table II. The frequency $f$ of the peak was calculated and is included for reference, since the damping varies with $f$.

Measurements of the frequency dependence of the linewidths were made for pure silica and LaSF-7. The frequency of the phonon peak can be varied by changing either the wavelength of the incident light or by changing the scattering angle. Wavelengths of 488 and 515 nm were used with scattering angles between 90 and 180°. For scattering angles much less than 180° the dispersion broadening can become as large as the intrinsic linewidth unless very small collection angles are used. In all cases, the dispersion broadening was carefully subtracted. Figure 4 shows a log-log plot of our measurements for the LA-phonon linewidth as a function of the peak frequency for pure silica and LaSF-7. Also included are the measurements of Pelous and Vacher[7] at frequencies of 24.7 and 33.8 GHz, and Pine[3] at 27.5 GHz. The slope of the log-log plot gives the exponent $m$ assuming $\gamma \alpha f^m$. In LaSF-7 $m = 1.1 \pm 0.3$, while in pure silica $m = 2.7 \pm 0.2$. Thus, the frequency dependence in

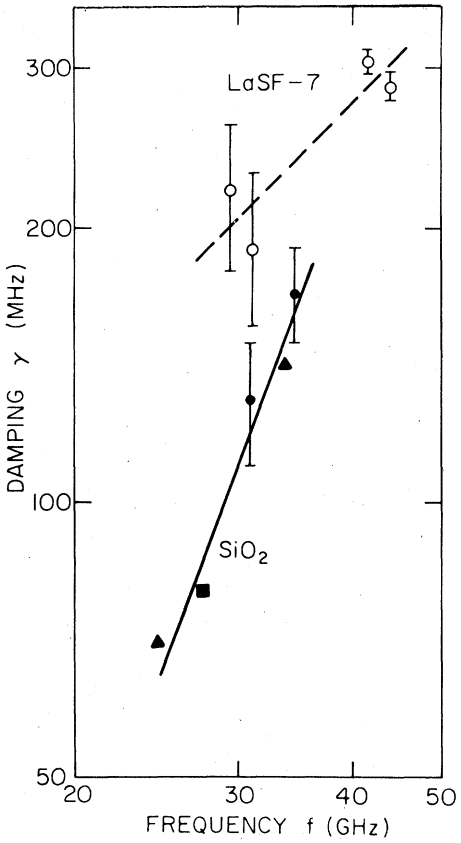


FIG. 4. Log-log plot of the full width at half maximum $\gamma$ of the longitudinal-acoustic peaks vs phonon peak frequency $f$ for pure silica and LaSF-7 glasses. For pure silica: solid triangles are from Ref. 7; the solid square is from Ref. 3; and the solid circles are from the present study. The open circles are results obtained here for LaSF-7. The solid straight line was fit to the pure silica data and has a slope of $m = 2.7 \pm 0.2$ while the dashed line was fit to the LaSF-7 data and has a slope of $m = 1.06 \pm 0.3$. The error bars are due to a ±5% deconvolution uncertainty, and a statistical uncertainty from many measurements.

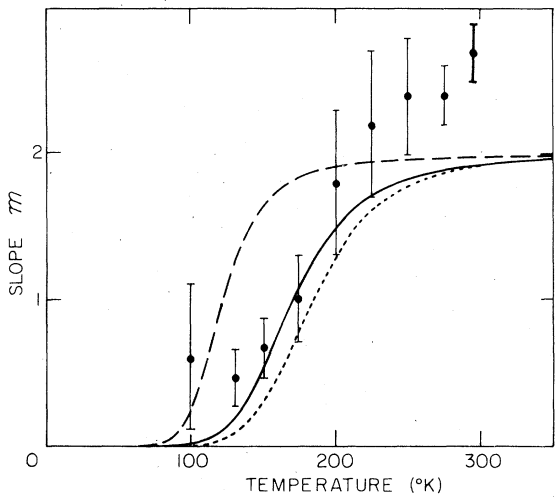


FIG. 5. Slope $m$ vs absolute temperature $T$. The calculated values for $m$ were determined from $\gamma \alpha f^m$ using the data of Ref. 3 and Ref. 7. The solid curve is a fit to Eq. (17) using the structural relaxation model of Anderson and Bommel (Ref. 18) using Arrhenius-type relaxation while the dotted curve uses the Eyring-type relaxation. The dashed line is derived using the anharmonic decay model of Pine (Ref. 3). The parameters for the structural relaxation model were derived from ultrasonic attenuation, while the anharmonic decay parameters are from hypersonic phonon linewidths.

silica is much stronger than in LaSF-7. The temperature dependence of the exponent $m$ in pure silica is shown in Fig. 5. The exponent is seen to decrease for decreasing temperature down to 100 °K.

## V. DISCUSSION

### A. Elastic and elasto-optic constants

The phonon peaks arising from transverse and longitudinal sound waves have been observed in glasses of varying composition. The only peak not observed was the TA peak in SF-6, which is attributed to a small elasto-optic constant. Huang *et al.*[26] have observed this peak by spontaneous Brillouin scattering. They determined the ratio $p_{12}/p_{44}$ as 4.8. Our results indicate that the lower limit for this ratio is 30. The longitudinal sound velocity measured in both experiments differ by only 2%, which is within experimental uncertainty. Although there is agreement for the LA peak, the discrepancy in the TA-peak intensity cannot be accounted for at this time.

The adiabatic and isothermal values of the shear modulus and Young's modulus showed no frequency dispersion for most of the glasses studied. Notable exceptions occured for BK-3, LaSF-7, and FK-51. In BK-3 the isothermal moduli were about 15% larger. In LaSF-7 and FK-51 the isothermal moduli were about 30 and 10% smaller, respectively. These discrepancies may result from sample differences.

The magnitude of the elasto-optic coefficients could not be correlated to the glass type or composition. Pure silica had one of the largest elasto-optic constants. The elasto-optic constant $p_{12}$ for all of the glasses varied only over a small range, 0.17 to 0.31. The constant $p_{44}$ varied over a much wider range, 0.014 to 0.083. The ratio $p_{12}/p_{44}$ varied from 3.4 to over 30 indicating that the polarizability change for shear and compressional strain are independent of each other.

### B. Acoustic-wave damping

The LA-phonon damping values in Table II are significantly larger than those found in crystalline materials. Glasses with similar composition show widely differing damping and there seems to be no correlation between the strength of this damping and other physical properties. Reference 24 gives the values for the size of the elastic scattering peak and the absolute Raman cross section for the same glasses studied here. Neither of these parameters are correlated to the damping. Comparisons are made difficult because the linewidths are registered at different frequencies. Since the frequency dependence varies considerably from $f^1$ in LaSF-7 to $f^2$ in pure silica it is difficult to remove this dependence without knowing the explicit dependence for each sample. The largest damping was found in LaSF-7 and FK-5 ($\gamma = 300$ MHz) whereas the smallest damping was observed in FK-51, a glass of composition similar to FK-5. The damping of these two fluorophosphate glasses were measured at similar frequencies. The linewidth of FK-51 is 50 MHz, which is a factor of 3 smaller than the next larger damping value. This anomalously small value is comparable to the damping in crystalline quartz at room temperature.[5] Raman scattering spectra confirm the amorphous nature of this glass.[24]

The damping in LaSF-7, $\gamma = 300$ MHz, is large compared to that in the other glasses. This material is known to have a central peak in the light-scattering spectrum having a width of 15 GHz (FWHM) at room temperature.[27] Extra degrees of freedom associated with this central peak may provide extra phonon decay channels which would explain the large damping in this glass. The Raman spectrum of LaSF-7 also shows a large light-scattering excess[28] between 0 and 20 $cm^{-1}$.[24] These extra degrees of freedom overlap the sound-wave frequencies and can also result in additional phonon broadening. The room-temperature damping has an almost linear frequency dependence. Two effects can give rise to an exponent of approximately $m = 1$; when the relaxation rate is comparable to the phonon frequency and, when there are two contributions, a frequency-independent part plus an equal contribution that varies as $f^2$. This latter process results when two relaxation mechanisms exist, one having a rate smaller than the phonon frequency and one whose rate is much larger. The mechanism causing the central peak is a candidate for the frequency-independent process. Alternately, it may be that the relaxation strength of the mechanism producing the central peak is small and only one mechanism contributes at these frequencies. Measurements on LaSF-7 show that the light scattering excess can be fit to a Lorentzian centered at zero frequency with a width of a few $cm^{-1}$ (Ref. 24) which is on the order of $\tau^{-1}$. This feature alone may give rise to a linear frequency dependence.

The five measurements of $\gamma(T)$, in pure silica, in Fig. 4 were obtained by three different researchers using different samples and different experimental apparatus. The good fit to a smooth curve is rather remarkable considering these differences and the uncertainty produced by the deconvolution process. A previous result gave $m = 2.2 \pm 0.2$ which overlapped the expected value of $m = 2.0$.[7] The exponent $m = 2.7 \pm 0.2$ derived in Fig. 4 indicates that there is a significant deviation. There are a number of reasons why the exponent could be smaller than $m = 2.0$ considering the model Eq. (16), although this model cannot be used to explain why $m > 2$ if $\tau$ is frequency independent. Anharmonic mechanisms can contribute to damping at high frequencies while not affecting it at low frequencies. If this is the case, a strong resonance is needed to explain the exponent deviation over this small frequency range.

Using the model parameters derived by Anderson and Bommel the structural relaxation model fits the experimental data much better than the anharmonic decay model with Pines parameters as indicated in Fig. 5. The quality of the fit indicates only that the parameters used in the particular model are more appropriate, since either model can give nearly the same curve by adjusting these parameters. The experimental values for $m$ are seen to be larger than 2.0 for the three highest temperatures.

## VI. CONCLUSIONS

The sound velocities of the glasses studied in this investigation were found to vary over a limited range of $3.5 \times 10^5$ to $6.9 \times 10^5$ cm/sec for longitudinal waves. The average ratio of the transverse to longitudinal velocities was found to be $v_{LA}/v_{TA} = 0.59 \pm 0.03$ for 15 glasses. This indicates that the shear and compressional restoring forces are closely related and are relatively independent of the glass forming network modifiers. The Pockels coefficients $p_{12}$ varied by only a factor of 2, while $p_{44}$ varied by a factor of 6, and the ratio $p_{12}/p_{44}$ varied by a factor 10 from one glass to another. This large variation is to be expected when the anisotropy of the polarization change resulting from macroscopic strain in dependent on the atomic glass network.

Values for the damping parameter $\gamma$ (FWHM) varied from 50 to 300 MHz with an average of $190 \pm 60$ MHz for all 16 glass samples. The effect of adding network modifiers to pure silica results in an almost negligible increase in $\gamma$ whereas within the other glass-type categories, such as phosphate and fluorophosphate, the damping is more dependent on the particular composition of the glass.

Damping models considering structural relaxation and anharmonic decay both predict frequency-dependent damping of the form $\gamma \alpha f^m$. Our results on LaSF-7 show $m \simeq 1$ which indicates that, at room temperature, the relaxation rate is approximately equal to the Brillouin frequency, $\tau^{-1} \simeq 1$ cm$^{-1}$. Results on pure silica show that $m = 2.7 \pm 0.2$ at room temperature, decreasing to $m = 1$ at 170° K, and decreases further below 170° K. Neither damping model predicts a value of $m > 2$ unless the relaxation rate is itself frequency dependent. These results indicate that a more detailed model of phonon damping in glasses is required to adequately describe the frequency dependence.

## ACKNOWLEDGMENTS

We would like to acknowledge Dr. A. J. Glass and Dr. M. J. Weber for providing sample materials and helpful discussions. We would also like to acknowledge the support of the U. S. DOE through Lawrence Livermore Laboratory Subcontract No. 7509105.

[1]R. S. Krishnan, Nature 165, 933 (1950).
[2]P. Flubacher, A. J. Leadbetter, J. A. Morrison, and B. P. Stoicheff, J. Phys. Chem. Solids 12, 53 (1959).
[3]A. S. Pine, Phys. Rev. 185, 1187 (1969).
[4]J. A. Bucaro and H. D. Dardy, J. Appl. Phy. 45, 5324 (1974).
[5]J. Pelous and R. Vacher, Solid State Commun. 18, 657 (1976).
[6]R. Vacher and J. Pelous, Phys. Lett. A 53, 233 (1975).
[7]J. Pelous and R. Vacher, Solid State Commun. 16, 279 (1975).
[8]L. D. Landau and E. M. Lifshitz, *Electrodynamics of Continuous Media* (Pergamon, New York, 1960), Chap. XIV.
[9]I. L. Fabelinskii, *Molecular Scattering of Light* (Plenum, New York, 1968).
[10]G. B. Benedek and K. Fritsch, Phys. Rev. 149, 647 (1966).
[11]W. P. Mason, in *American Institute of Physics Handbook* (McGraw-Hill, New York, 1972), Sec. 3.
[12]G. E. Durand and A. S. Pine, IEEE J. Quantum Electron. 4, 523 (1968).
[13]P. A. Fleury and P. D. Lazay, Phys. Rev. Lett. 26, 1331 (1971).
[14]P. A. Fleury, J. Acoust. Soc. Am. 49, 1041 (1971).
[15]H. E. Bommel and K. Dransfeld, Phys. Rev. 117, 1245 (1960).
[16]A. Akheizer, J. Phys. (Moscow) 1, 277 (1939).
[17]S. Brawer, Phys. Chem. Glasses 16, 2 (1975).
[18]O. L. Anderson and H. E. Bommel, J. Am. Ceram. Soc. 38, 125 (1955).
[19]J. Jäckle, L. Piché, W. Arnold, and S. Hunklinger, J. Non-Cryst. Solids 20, 365 (1976).
[20]J. R. Sandercock, in *Light Scattering in Solids*, edited by M. Balkanski (Flammarion, Paris, 1971).
[21]J. Schroeder, R. Mohr, P. B. Macedo, and C. J. Montrose, J. Am. Ceram. Soc. 56, 510 (1973).
[22]K. Vedam, Phys. Rev. 78, 472 (1950).
[23]W. Primack and D. Post, J. Appl. Phys. 30, 779 (1959).
[24]D. Heiman, R. W. Hellwarth, and D. S. Hamilton, J. Non-Cryst. Solids (to be published).
[25]D. Heiman and S. Ushioda, Phys. Rev. B 17, 3616 (1978).
[26]Y. Y. Huang, J. L. Hunt, and J. R. Stevens, J. Appl. Phys. 44, 3589 (1973).
[27]P. A. Fleury and K. B. Lyons, Phys. Rev. Lett. 36, 1188 (1976).
[28]G. Winterling, Phys. Rev. B 12, 2432 (1975).
[29]G. W. Morey, *The Properties of Glass* (Reinhold, New York, 1954).